

Communication

Enhanced Electrochemical Performance of Supercapacitors via Two-Dimensional Indium Sulfide Heterostructure on Carbon Nanotubes

Niraj Kumar ^{1,†}, Dhananjay Mishra ^{1,†}, Ajit Kumar ¹, Bidyashakti Dash ¹, Rajneesh Kumar Mishra ^{2,*}, Junyoung Song ^{1,*} and Sung Hun Jin ^{1,*}

¹ Department of Electronics Engineering, Incheon National University, Incheon 22012, Republic of Korea

² Department of Physics, Yeungnam University, Gyeongsan 38541, Republic of Korea

* Correspondence: rajneeshmishra08@gmail.com (R.K.M.); jun.song@inu.ac.kr (J.S.); shjin@inu.ac.kr (S.H.J.); Tel.: +82-32-835-8865 (S.H.J.)

† These authors contributed equally to this work.

Abstract: This study reports on the synthesis and characterization of a novel electrode material for supercapacitor applications based on a clustered heterostructure of indium sulfide (In_2S_3) and single-walled carbon nanotubes (SWCNTs). The In_2S_3 -SWCNT (INSC) sample was prepared using the facile successive ionic layer adsorption and reaction (SILAR) method and demonstrated a higher specific capacitance (258 Fg^{-1} at 1 Ag^{-1}) compared to the bare indium sulfide (In_2S_3) electrode. The enhanced electrochemical performance is attributed to the synergistic effect between the In_2S_3 and SWCNTs, which improves electron transportation, catalytic nature, and specific capacitance. Moreover, the cyclic stability of the INSC electrode was significantly improved, retaining 96.8% of the initial capacitance after 3000 cycles. The high voltage holding capacity and high cyclic efficiency of the fabricated INSC-based supercapacitor devices suggest their potential for next-generation energy storage devices. Additionally, the INSC electrode-based supercapacitor devices exhibit excellent flexibility and bendability, retaining similar performance even at a bending angle of 180° , making them suitable for flexible energy storage applications.

Keywords: 2D materials; In_2S_3 nanostructure; SILAR deposition; supercapacitor



Citation: Kumar, N.; Mishra, D.; Kumar, A.; Dash, B.; Mishra, R.K.; Song, J.; Jin, S.H. Enhanced Electrochemical Performance of Supercapacitors via Two-Dimensional Indium Sulfide Heterostructure on Carbon Nanotubes. *Appl. Sci.* **2023**, *13*, 3678. <https://doi.org/10.3390/app13063678>

Academic Editor: Antonio Di Bartolomeo

Received: 10 February 2023

Revised: 9 March 2023

Accepted: 11 March 2023

Published: 14 March 2023



Copyright: © 2023 by the authors. Licensee MDPI, Basel, Switzerland. This article is an open access article distributed under the terms and conditions of the Creative Commons Attribution (CC BY) license (<https://creativecommons.org/licenses/by/4.0/>).

1. Introduction

Recently, supercapacitors (SCs) with high performance, such as higher specific capacitance, faster charging and discharging, and a sustainable cyclic lifespan, have become highly necessary owing to the rapidly growing market for wearable electronics. The bendability and sustainable performance of the SCs are essential features in wearable devices. The design of novel electrode materials and assembly of the SCs could be the strategy to provide sufficient flexibility in the SCs. Transition metal sulfides (TMSs) have been attractive for SC applications due to their excellent conductivity, mechanical robustness, thermal stability, and great redox reaction activity [1,2]. As a prominent TMS nanomaterial, indium sulfide (In_2S_3) could be chosen as an excellent electrode material as it possesses a layered structure with stable structural form and high electrical conductivity [3]. In our previous report, In_2S_3 was prepared as an electrode material via a solvothermal method. However, the solvothermal method involves high temperatures during synthesis, and thereby, when adopted for the direct growth of electrode materials, NF substrates often become brittle, limiting their durability and adaptability in wearable applications [4]. Recently, 2D layered nanostructure materials have been the focus of research towards advanced electrode materials as they have a high surface-interface area, facilitating better electrochemical kinetics and charge storage. However, the material's stability in itself is a major concern for its applicability as an electrode material.

SWCNTs are well explored toward enhancing the mechanical robustness and providing an efficient charge transfer channel, leading to more exposure of active sites while decreasing the risk of stacking or aggregation. Herein, we report the bare NF and SWCNTs-In₂S₃ heterostructure-based electrode materials prepared by a facile, room-temperature successive ionic layer adsorption and reaction (SILAR) method. This room-temperature synthesis route yields the layered SWCNT-In₂S₃ heterostructure directly grown on NF, which enables it to accommodate better robustness and flexibility. Furthermore, the SILAR method has benefits for controlling minute film thickness due to the consequential nature of film growth [5].

Here, we report (i) SWCNTs incorporated into a 2D In₂S₃ network heterostructure via a SILAR method of growth for SC applications, (ii) higher electrochemical performance of the SWCNT-In₂S₃ heterostructure in terms of specific capacitance, excellent cyclic retention, and unvarying performance even in 180° bending, demonstrating remarkable flexibility. (iii) Also, commercial reliability is tested by voltage holding, leakage current, and self-discharge. Interestingly, our SWCNTs incorporated into a 2D In₂S₃ heterostructure exhibited outstanding electrochemical performance, excellent cyclic stability, and 180° mechanical flexibility. Furthermore, the voltage holding capability, high cyclic efficiency, and operating power range of fabricated SSC devices demonstrate that the prepared electrode material can be an excellent candidate for next-generation energy storage devices.

2. Materials and Methods

The binder-free In₂S₃-SWCNT heterostructure-based electrodes were grown on NF by utilizing a two-step cyclic SILAR deposition method. All the chemicals utilized were of analytical grade and were used without any further treatment or purification. The chemicals indium chloride pentahydrate and thiourea were purchased from Sigma Aldrich (St. Louis, MI, USA). The single-walled carbon nanotube solutions (SWCNT) were procured from KH Chemicals Inc. The average diameter and length of SWCNT were 1.1–1.4 nm and 5 μm, respectively, with a G/D ratio of more than 100 [6]. The detailed method for electrode synthesis is as follows: A two-step cyclic SILAR process is employed for the deposition of electrode material. As a typical procedure for a one-cycle SILAR process, in which the nickel foam substrate (NF) was first immersed in an anion-rich solution (0.05 M Na₂S) and then immersed in a solution containing metal precursors (0.05 M) as the cationic source. This was followed by a dip in DI water in a beaker (25 mL volume) to remove any loosely bound corpuscles from the substrate. In each beaker, an NF substrate was dipped for 30 s after the previous beaker, and 20 cycles with the same methods were repeated consecutively for homogeneous, binder-free deposition on the surfaces of the substrates. Following that, the samples were dried in an oven at 60 °C for 12 h. For composite material preparation, one more beaker (1 mL SWCNT in 25 mL water) is kept between each SILAR cycle (after DI water).

2.1. Fabrication of an SSC Device

For the fabrication of solid-state symmetric (SSC) devices, a material-coated electrode sample on a NF substrate with a deposition area of (2 × 3) cm² was used. Three grams of PVA and three grams of potassium hydroxide were dissolved in thirty milliliters of deionized water to form a semi-solid electrolyte gel. Using 0.45-micron filter paper (Millipore) (procured from Merck Millipore) as a separator, the electrodes were sandwiched together and held at room temperature for two minutes after being soaked in electrolyte gel for two minutes. A protective coating of paraffin film is applied to the fabricated SSC device to prevent leaking and short-circuiting, and it is allowed to solidify at room temperature overnight to ensure optimal operation.

2.2. Characterization Techniques

The X-ray Diffraction (XRD) measurements were performed on a Rigaku SmartLab [Cu K] radiation (1.54 Å) source. The morphology of as-synthesized electrode material and EDS (energy-dispersive X-ray spectroscopy) were investigated using the JEOL/JSM-7800F field emission scanning electron microscopy instrument. The FTIR spectra for electrode material on NF substrate were acquired using an FT-IR microscope, the Hyperion 2000. Electrochemical studies on a fabricated two-terminal supercapacitor device were carried out using an IVIUM Technologies Compactstat.h electrochemical workstation. On NF, the mass loadings on INS and INSC are 1.8 and 2.2 mg/cm², respectively. The electrochemical performance of prepared, direct-grown electrode samples was investigated using cyclic voltammetry (CV), galvanostatic charge-discharge (GCD), and electrochemical impedance spectroscopy (EIS) techniques.

The following equation can be used to determine the specific capacitance (C_s) of electrode samples based on CV curves [7].

$$C_s = \frac{1}{ms(V_2 - V_1)} \int_{V_1}^{V_2} I(V)dv \quad (1)$$

where “m” denotes the mass of electrode material deposited on the substrate as determined by the mass difference method, “s” denotes the scan rate, “I(V)” denotes the response current, and “(V₂ – V₁)” denotes the measurement potential window.

The specific capacitance can be determined from the GCD study.

$$C_s = Q/(\Delta V \times m) = (I \times \Delta t)/(\Delta V \times m) \quad (2)$$

I, Δt, ΔV, and m denote the utilized current, discharge time, accepted potential window of the GCD curve, and active mass deposited on the substrate.

The following formulae are utilized to calculate both parameters, energy density and power density, from GCD curves.

$$E = 1/2(C_s \times V_{max}^2) \quad (3)$$

$$P = (E \times 3600)/\Delta t \quad (4)$$

V_{max} , E, and P are used to denote the maximum voltage, energy density, and power density, respectively.

3. Results and Discussion

A schematic representation of the SILAR process for the preparation of electrode materials is depicted in Figure 1a. INS nanostructures with stratified, yet interconnected clumps resembling tree reef corals' morphology are shown in Figure 1b, grown on NF. On the other hand, INSC grown on NF substrate with an even more integrated layered clump nanostructure exhibiting cauliflower-like morphology is shown in Figure 1c. This SWCNT can improve the electrode surface properties, charge transport, and performance consistency of the electrode sample. The well-separated layered nanostructure enables better electrochemical reactions and provides a higher active electrode surface area than the as-prepared electrode samples.

The Substrate Preparation: The substrate is first cleaned and dried to remove any impurities or contaminants from its surface. This is important to ensure that the deposited film adheres well to the substrate.

Immersion in the Precursor Solution: The substrate is then immersed in a precursor solution containing a dissolved metal or metal compound. The substrate is kept in the solution for a predetermined amount of time to allow the precursor ions to adsorb onto its surface. In our case, the indium precursor is attached to the substrate via physical adsorption, which is mainly driven by Vander Waals force.

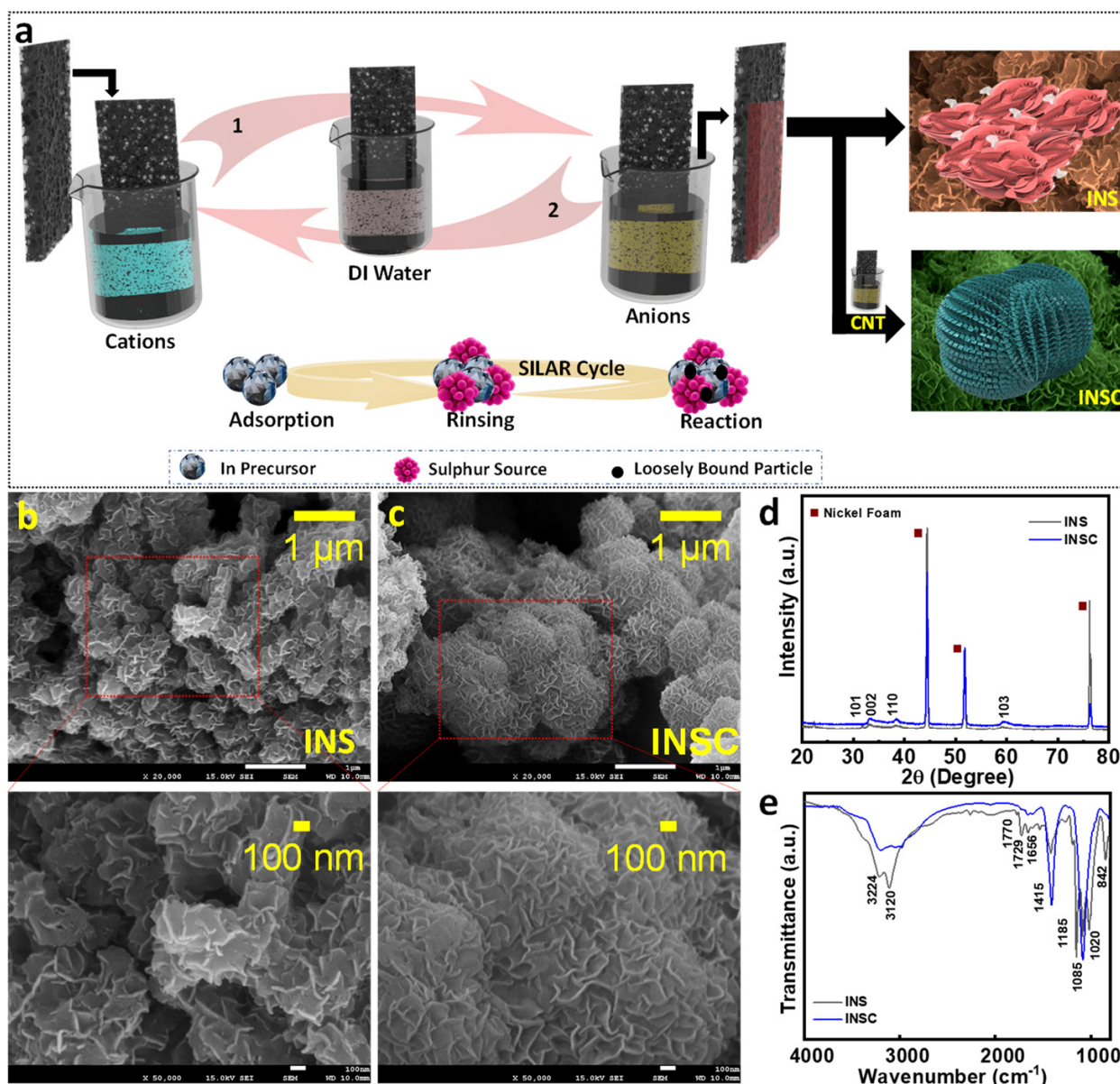


Figure 1. (a) Schematic illustration of synthesis of sample INS and INSC, FE-SEM images of sample (b) INS, (c) INSC, (d) XRD pattern (missing is the JCPDS file), and (e) FTIR spectra of as-prepared electrode materials INS and INSC.

Rinsing: After the adsorption step, the substrate is rinsed with a suitable solvent to remove any excess precursor solution that may be on its surface.

Reaction: The rinsed substrate is then immersed in a second solution (a sulfide dioxide precursor), typically a reducing agent, which reacts with the adsorbed precursor ions to form a thin film of the desired material on the substrate surface. The reducing agent reacts with the precursor ions in a controlled manner to ensure the growth of a uniform and conformal film.

Drying: Finally, the substrate is dried to remove any remaining solvent or water molecules, leaving behind a thin film of the desired material on its surface.

XRD (X-ray diffraction) was used to examine the crystalline phase structure of both electrode materials, and the resulting spectra are shown in Figure 1d (Standard ICDD pattern 32-0456), which corresponds to the cubic structure of In_2S_3 , which is found in the XRD spectrum of prepared samples [8]. In spectra, Miller indices are used to index all peaks. All peak positions have confirmed a cubic phase of In_2S_3 consistent with previously

reported values. The molecular structure and functional group present in In_2S_3 were analyzed using the FTIR (Fourier-transform infrared spectroscopy) spectra, as shown in Figure 1e. The vibration of the O-H groups in chemisorbed water molecules is characterized by a broad peak near 3224 cm^{-1} , the bending vibration of H_2O occurs at 1656 cm^{-1} , and the sulfonic group is characterized by signature peaks between 800 and 1500 cm^{-1} [9].

3.1. Electrochemical Characterization

In Figure 2a, the electrochemical performance of the as-synthesized electrode materials (INS and INSC) is compared via cyclic voltammetry (CV) curves at a fixed scan rate of 100 mVs^{-1} . The INSC-based sample exhibits a larger enclosed area under the CV curve than the INS sample, indicating better electrochemical kinetics [10]. The calculated specific capacitance values of INS and INSC at various scan rates ranging from 10 mVs^{-1} to 100 mVs^{-1} , are shown in Figure 2b. The normalized CV curves for INS and INSC are compared in Figure S9, which shows clearly the increase in enclosed area under the CV curve for INSC compared to INS [11–13]. Notably, the obtained specific capacitance for the INSC sample (210 Fg^{-1}) is significantly higher than the bare INS (112.7 Fg^{-1}), which clearly shows the effect of the SWCNT framework [6]. This improvement in the specific capacitance of INS with SWCNT heterostructure is attributed to the improved usage of redox species, enhancement of electrochemically available active sites, and quick charge transfer kinetics. The synergistic and cooperative contribution of SWCNT with INS materials boosted dopant (counter-anions) diffusion and improved conducting pathways for better electrolyte accessibility, which may be the reason for boosted electrochemical performance [14]. The CV measurements of the INSC-fabricated SSC device (Figure 2c) were performed at various potential windows ranging from 0.6 to 1.2 V , leading to an increase in the active integrated area under the curve. By scanning the CV data at various potential windows, the behavior of the supercapacitor is estimated under different operating conditions. For example, scanning at a wider potential window provides information on the capacitance and energy density of the device at high voltages, while scanning at a narrower potential window can reveal the capacitance and power density at low voltages. Overall, scanning the CV data of an INSC-based SSC device at various potential windows provides valuable information on its performance characteristics, leading to the optimization of its design for specific applications.

Figure 2d shows comparative galvanostatic charge-discharge (GCD) curves for INS and INSC samples. Higher discharge times observed in sample INSC (258 Fg^{-1}) show better capacitance performance and match the CV result. Figure 2e shows the calculated specific capacitance values of the sample at different current densities. Figure 2f shows GCD curves of sample INSC at different potential windows, ranging from 0.6 to 1.6 V , indicating the wide operating area of the prepared SSC device. Redox reactions in the presence of hydroxide counter-electrolyte anions can be formulated as follows for the ionic charge storage behavior of In_2S_3 [4].

SWCNTs possess unique electronic, optical, and mechanical properties, making them a popular component in heterostructures. Incorporating SWCNTs into an In_2S_3 (INS) heterostructure can lead to various effects, such as band alignment, charge transfer, optical properties, and mechanical properties. The resulting enhancement in the electrochemical performance and mechanical stability of INS in the heterostructure is significant.

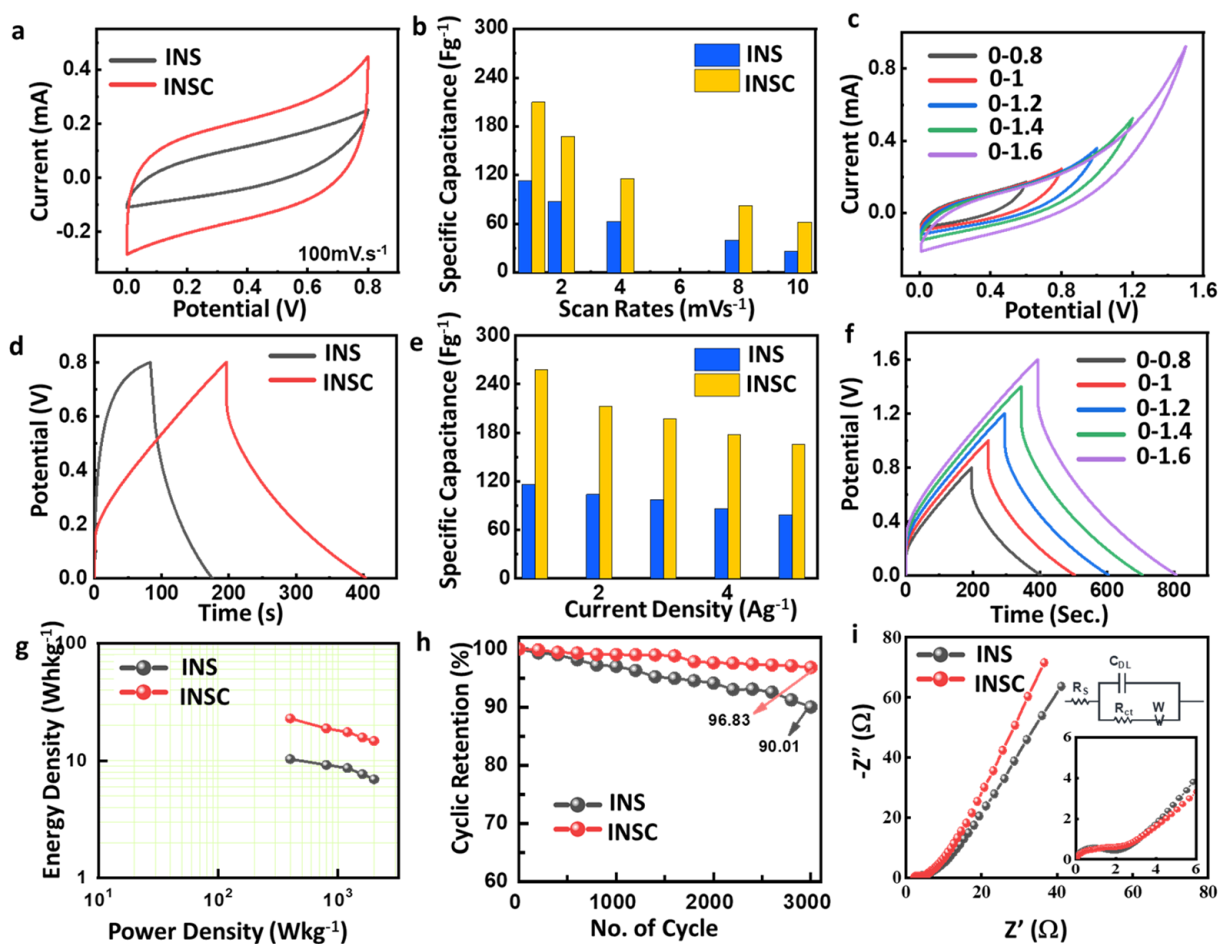


Figure 2. (a) Comparative CV curves at a scan rate of 100 mVs^{-1} ; (b) extracted specific capacity values at various scan rates; (c) CV curve at the various potential windows at a scan rate of 100 mVs^{-1} ; (d) comparative GCD curves; (e) extracted specific capacity values at various current densities; (f) GCD curve at the various potential windows; (g) Ragone plot; (h) cyclic stability spectra; and (i) Nyquist plot of sample INS and INSC.

The electronic properties of the heterostructure can be influenced by the SWCNTs' band alignment, which creates a built-in electric field that affects the flow of charge carriers. Furthermore, the high mechanical strength and flexibility of SWCNTs can improve the durability and flexibility of the device. The SWCNTs can also interact with INS through charge transfer, which can alter the electronic properties of the device and the valence state of the materials. The effect of SWCNTs on the valence state of the INS heterostructure is complex and dependent on various factors, including the nature of the interaction, the energy level alignment between the materials, relative positions in the heterostructure, and the chemical properties of the materials. According to density functional theory (DFT) analysis, the work function of SWCNTs is higher than that of In_2S_3 , resulting in a downward band bending at the interface and a potential barrier for electron transfer. However, the study found that the barrier height is relatively low, allowing for efficient electron transfer across the heterojunction [15].

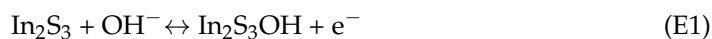


Figure 2g illustrates the Ragone plot (a graph between power density and energy density) of samples INS and INSC. For SC applications, the Ragone plot can analyze the functionalities and operational material efficiency [16]. Sample INSC exhibits a high energy density of 22.93 Whkg^{-1} at a power density of 400 Wkg^{-1} . CV measurements

at 5 mVs^{-1} were performed to evaluate its cyclic stability (Figure 2h) for 3000 cycles. Interestingly, sample INSC (96.8%) displays outstanding cyclic retention compared to the INS sample (90%). Swelling and shrinkage are speculated to be two main factors that influence the stability of electrode materials. Thus, significant enhancement of cyclic stability is attributed to SWCNTs enabling physical reinforcement, leading to a robust morphology of the heterostructure. In addition, the insertion of SWCNTs into electrode materials significantly increases the stability behaviors of the electrodes by forming π - π bonds [17]. This increases the number of active sites and creates a more conductive channel, allowing greater electrode-electrolyte interaction. SWCNTs establish cross-linking with layers, which increases conductivity and, as a result, improves the electrochemical performance [18].

Electrochemical impedance spectroscopy (EIS) is used to examine the charge transfer and estimate the impedance parameters of the electrode material. Figure 2i shows that the EIS spectra of the fabricated SSC device range from 100 kHz to 0.01 Hz with a bias voltage of 0.1 V. The nearly identical shape of the EIS curves implies that the charge is channelized comparably in each material sample. A smaller semicircle, smaller intercept, and more vertical line toward the low-frequency side suggest a greater mass transfer limit, faradic charge transport, and reduced inter-facial charge resistance in the sample INSC. The estimated impedance parameters for both the electrode samples are tabulated in Table S2 in Supporting Information.

3.2. Self-Discharge Study

Self-discharge (SD) behavior and voltage holding (VH) capabilities are essential performance factors to consider when evaluating the applicability of supercapacitors for practical applications. After charging, the rapid self-discharging of SCs limits their employability on an industrial scale. Figure 3a shows four 100-cycle GCD measurements for SSC devices from INSC samples, followed by 2 h VH and 2 h SD tests. Figure 3b shows a sequence of GCD (100 cycles), followed by a 2-h VH test for an INSC SSC device. The GCD cycling was done at 1 Ag^{-1} from 0 to 1.2 V, and furthermore, VH tests were performed at 1.2 V for 2 h, and SD tests were performed at OCP (open circuit potential), that is, in floating condition. Over two hours, a four-cycle VH test showed almost no internal resistance at the device level. Resistance and diffusion charge redistribution are important factors determining SD in SC devices [19]. The device was examined for SD, VH, and leakage currents, and the results showed that SD mitigation was due to improved nanostructural integrity in the fabricated SSC device. We exhibited a fabricated SSC device for LED illumination to further validate its practical application.

Two SSC devices, connected in series, are extremely efficient when used to illuminate red commercial LED lights (Figure 3c). The charge transfer behavior of ions in a layered nanostructure for charge storage is depicted in the scheme in Figure 3d. Excellent electrochemical performances may indeed result from (i) a well-defined layer structure; (ii) the provision of highly accessible interfacial contacts due to the layered facets of 2D In_2S_3 , which allows for greater use of the ion accumulation; and (iii) decreased internal material resistance due to the incorporation of conducting SWCNTs, which results in a shorter electron diffusion length during the charge/discharge process [20]. All electrochemical results substantially support the merits of the developed heterostructure embedded with INSC electrode material as a high-performance supercapacitor application.

Mechanical flexibility testing is a crucial step in ensuring the overall performance, robustness, and longevity of a device. This study evaluates the ability of the SC device to maintain its functionality under various bending angles. In particular, the mechanical flexibility testing was performed on a SSC device, and the results are shown in Figure 4a–e. For comparing the electrochemical performance, the CV curves of the SSC device were plotted in Figure 4f at a scan rate of 100 mVs^{-1} , which revealed the capacitance performance of the device. Essentially, it was observed that the capacitance performance of the SSC

device did not degrade even when the bending angle was increased from 0° to 180°, which is a significant deviation from the flat (0°) condition.

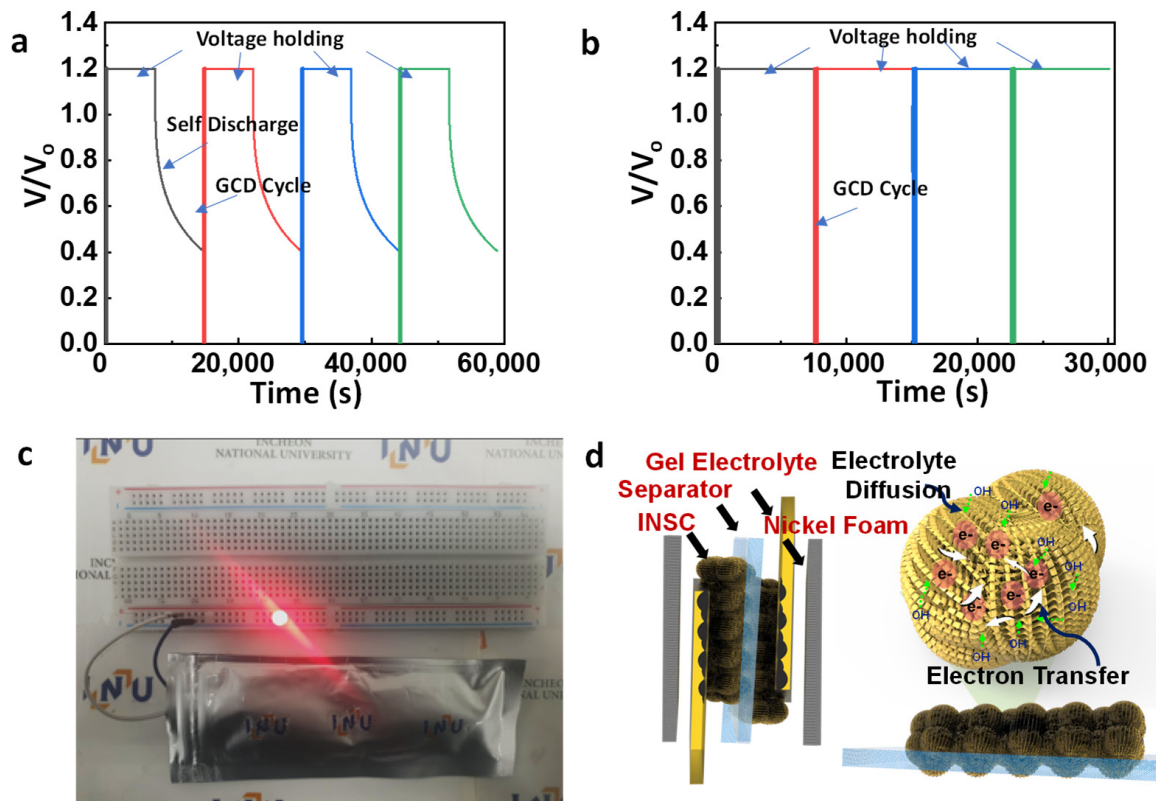


Figure 3. (a) GCD (100 cycles) + VHT (2 h) + SD (2 h); (b) GCD (100 cycles) + VHT (2 h) for an INSC-based SSC device; (c) demonstration of commercial red LED illumination; and (d) schematic artwork for illustrating electron transmission at the electrode-electrolyte interface in a fabricated symmetric supercapacitor.

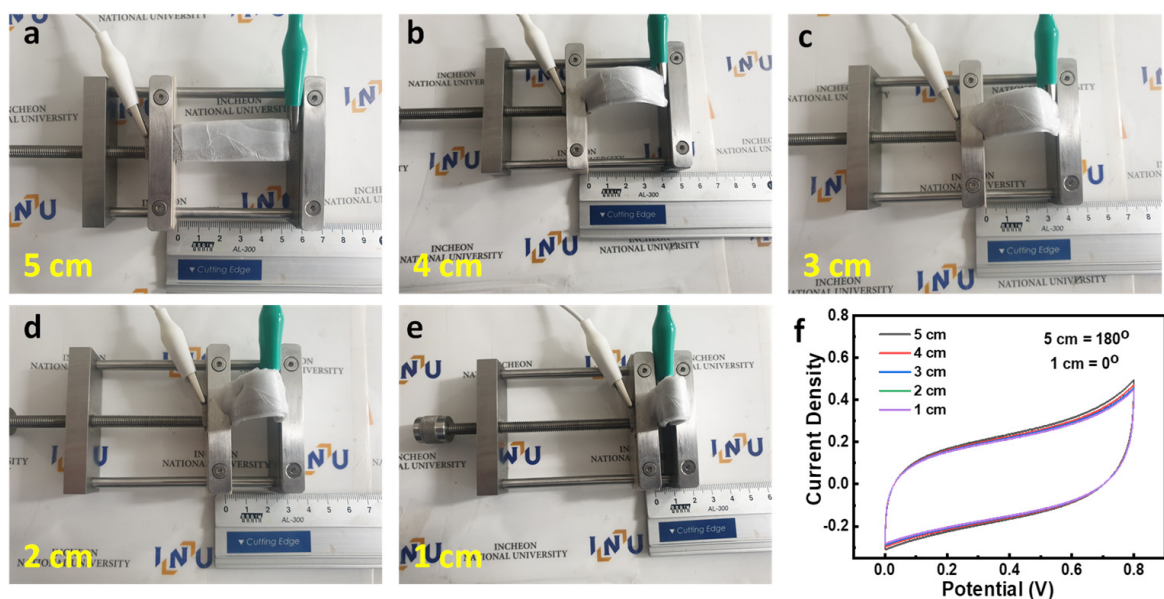


Figure 4. (a–e) Mechanical testing of a fabricated SSC device at various bending states and (f) the corresponding CV graph for a fabricated INSC-based SSC device.

This finding demonstrates the excellent flexible nature of the fabricated INSC-based SSC device and indicates that the device's capacitance performance remains unaffected even under extreme bending conditions. This, in turn, ensures the device's long-term durability and robustness, as it can maintain its functionality even in challenging environments. Thus, the test of mechanical flexibility plays a vital role in evaluating the performance, robustness, and longevity of a device. The results of the mechanical flexibility testing performed on the MSC device show that it has excellent flexible properties and does not degrade even under extreme bending conditions, making it an ideal choice for applications that require flexibility and robustness.

4. Conclusions

The newly developed 2D In_2S_3 heterostructure electrode material exhibits high capacitance, high power density, and exceptional cycle retention properties. INSC heterostructure offers efficient charge transfer and a stable structure with increased active sites and reduced stacking or aggregation, contributing to its impressive electrochemical and stability performance. The 2D INSC material demonstrates its potential as a next-generation electrode material for supercapacitor applications, offering improved performance and stability over traditional electrode materials. The results suggest this material could be used in energy storage and power conversion systems. Overall, the 2D In_2S_3 heterostructure is a promising option for supercapacitor applications due to its high capacitance, power density, and cycle retention properties.

Supplementary Materials: The following supporting information can be downloaded at: <https://www.mdpi.com/article/10.3390/app13063678/s1>. Figure S1: EDAX color mapping image of INS and INSC samples; Figure S2: EDAX spectra of (a) INS and (b) INSC samples; Figure S3: CV curves at different scan rates (10 mVs^{-1} to 100 mVs^{-1}) of (a) INSC and (b), INSC-based SCs; Figure S4: 2T GCD curves at different scan rates (1 Ag^{-1} to 100 Ag^{-1}) of sample (a) INSC and (b), INSC; Figure S5. CV curves at different scan rates (10 mVs^{-1} to 100 mVs^{-1}) of (a) INSC and (b) INSC-based SCs; Figure S6. 2T GCD curves of sample INSC at (a) lower scan rates (1 Ag^{-1} to 5 Ag^{-1}) and (b) a higher scan rate range (1 Ag^{-1} to 100 Ag^{-1}); Figure S7. Comparative CV curves of bare SWCNT and INSC in a potential window of 1.2 V; Figure S8. EIS test before and after the stability test; Figure S9. Normalized CV curves for INS and INSC samples at a scan rate of 100 mVs^{-1} ; Table S1. Comparison between previously published indium electrode materials and the current work on electrochemical properties [4,21–28]; Table S2. Impedance parameters estimated from the Nyquist plot of sample INS and INSC.

Author Contributions: Conceptualization, N.K., D.M. and S.H.J.; methodology, N.K. and B.D.; software, D.M. and A.K.; validation, D.M., R.K.M. and S.H.J.; formal analysis, N.K.; investigation, B.D.; resources, J.S. and S.H.J.; data curation, N.K., D.M.; writing—original draft preparation, N.K., D.M. and S.H.J.; writing—review and editing, D.M. and S.H.J.; visualization, D.M.; supervision, J.S. and S.H.J.; project administration, J.S. and S.H.J.; funding acquisition, R.K.M., J.S. and S.H.J. All authors have read and agreed to the published version of the manuscript.

Funding: This research was funded by the Post-Doctoral Research Program (2018) through Incheon National University (INU), Incheon, Republic of Korea.

Data Availability Statement: No new data were created.

Conflicts of Interest: The authors declare no conflict of interest.

References

1. Geng, P.; Zheng, S.; Tang, H.; Zhu, R.; Zhang, L.; Cao, S.; Xue, H.; Pang, H. Transition Metal Sulfides Based on Graphene for Electrochemical Energy Storage. *Adv. Energy Mater.* **2018**, *8*, 1703259. [CrossRef]
2. Kulkarni, P.; Nataraj, S.K.; Balakrishna, R.G.; Nagaraju, D.H.; Reddy, M.V. Nanostructured Binary and Ternary Metal Sulfides: Synthesis Methods and Their Application in Energy Conversion and Storage Devices. *J. Mater. Chem. A* **2017**, *5*, 22040–22094. [CrossRef]
3. Li, Q.; Wang, Z.; Zhang, Y.; Hu, P.; Wang, T.; Yun, F. Indium Tin Oxide Nanowires as Voltage Self-Stabilizing Supercapacitor Electrodes. *J. Mater. Res.* **2019**, *34*, 3195–3203. [CrossRef]

4. Kumar, N.; Mishra, D.; Yeob Kim, S.; Na, T.; Hun Jin, S. Two Dimensional, Sponge-like In₂S₃ Nanoflakes Aligned on Nickel Foam via One-Pot Solvothermal Growth and Their Application toward High Performance Supercapacitors. *Mater. Lett.* **2020**, *279*, 128467. [[CrossRef](#)]
5. Kumar, N.; Mishra, D.; Kim, S.Y.; Jin, S.H. Two Dimensional, Bi-Layered SnS₂@Co₃S₄ Heterostructure Formation via SILAR Method: Toward High Performance Supercapacitors with Superior Electrodes. *Mater. Lett.* **2020**, *262*, 127173. [[CrossRef](#)]
6. Seo, S.G.; Baek, J.L.; Mishra, D.; Jo, H.; Kwon, H.-I.; Jin, S.H. One-Pot Hydrothermal Growth of Indium Oxide-CNT Heterostructure via Single Walled Carbon Nanotube Scaffolds and Their Application toward Flexible NO₂ Gas Sensors. *J. Alloy. Compd.* **2022**, *922*, 166169. [[CrossRef](#)]
7. Mirzaee, M.; Pour, G.B. Design and Fabrication of Ultracapacitor Based on Paper Substrate and BaTiO₃/PEDOT: PSS Separator Film. *Recent Pat. Nanotechnol.* **2018**, *12*, 192–199. [[CrossRef](#)]
8. Nayak, A.K.; Lee, S.; Sohn, Y.; Pradhan, D. Synthesis of In₂S₃ Microspheres Using a Template-Free and Surfactant-Less Hydrothermal Process and Their Visible Light Photocatalysis. *CrystEngComm* **2014**, *16*, 8064–8072. [[CrossRef](#)]
9. Zhang, X.; Shao, C.; Li, X.; Lu, N.; Wang, K.; Miao, F.; Liu, Y. In₂S₃/Carbon Nanofibers/Au Ternary Synergetic System: Hierarchical Assembly and Enhanced Visible-Light Photocatalytic Activity. *J. Hazard. Mater.* **2015**, *283*, 599–607. [[CrossRef](#)]
10. Mishra, D.; Yeob Kim, S.; Hun Jin, S. Hierarchically-Formed Nickel Sulfide Heterostructure via SILAR on Hydrothermally Grown Cobalt Oxide Scaffolds: Role of Number of Over-Coating and Evolution of Electrochemical Performance in Supercapacitor Electrodes. *Appl. Surf. Sci.* **2021**, *564*, 150436. [[CrossRef](#)]
11. Stark, J.E.; Allison, A.; Andreas, H.A. Cyclic Voltammetry of Porous Carbon Is Impacted by Charge Redistribution—Understanding the Mechanism and Effects on Performance Metrics. *Carbon* **2020**, *170*, 245–255. [[CrossRef](#)]
12. Zhao, Z.; Zhang, W.; Liu, M.; Wang, D.; Wang, X.; Zheng, L.; Zou, X.; Wang, Z.; Li, D.; Huang, K.; et al. Switching Optimally Balanced Fe–N Interaction Enables Extremely Stable Energy Storage. *Energy Environ. Mater.* **2022**, 1–9. [[CrossRef](#)]
13. Peng, C.; Jin, M.; Han, D.; Liu, X.; Lai, L. Structural Engineering of V₂O₅ Nanobelts for Flexible Supercapacitors. *Mater. Lett.* **2022**, *320*, 132391. [[CrossRef](#)]
14. Yang, M.Q.; Weng, B.; Xu, Y.J. Synthesis of In₂S₃-CNT Nanocomposites for Selective Reduction under Visible Light. *J. Mater. Chem. A* **2014**, *2*, 1710–1720. [[CrossRef](#)]
15. He, Z.; Wang, Y.; Dong, X.; Zheng, N.; Ma, H.; Zhang, X. Indium Sulfide Nanotubes with Sulfur Vacancies as an Efficient Photocatalyst for Nitrogen Fixation. *RSC Adv.* **2019**, *9*, 21646–21652. [[CrossRef](#)]
16. Le, T.S.; Truong, T.K.; Huynh, V.N.; Bae, J.; Suh, D. Synergetic Design of Enlarged Surface Area and Pseudo-Capacitance for Fiber-Shaped Supercapacitor Yarn. *Nano Energy* **2020**, *67*, 104198. [[CrossRef](#)]
17. Kim, A.Y.; Senthil, T.S.; Kwak, B.S.; Kang, M. Improved Photovoltaic Efficiency on TiO₂/In₂S₃ Double Layered Electrodes. *Mater. Chem. Phys.* **2015**, *149*, 302–308. [[CrossRef](#)]
18. Wu, H.; Guo, J.; Yang, D. Facile Autoreduction Synthesis of Core-Shell Bi-Bi₂O₃/CNT with 3-Dimensional Neural Network Structure for High-Rate Performance Supercapacitor. *J. Mater. Sci. Technol.* **2020**, *47*, 169–176. [[CrossRef](#)]
19. Bello, A.; Barzegar, F.; Madito, M.J.; Momodu, D.Y.; Khaleed, A.A.; Masikhwa, T.M.; Dangbegnon, J.K.; Manyala, N. Stability Studies of Polypyrrole- Derived Carbon Based Symmetric Supercapacitor via Potentiostatic Floating Test. *Electrochim. Acta* **2016**, *213*, 107–114. [[CrossRef](#)]
20. Li, H.; Liang, J. Recent Development of Printed Micro-Supercapacitors: Printable Materials, Printing Technologies, and Perspectives. *Adv. Mater.* **2020**, *32*, e1805864. [[CrossRef](#)]
21. Tuzluca, F.N.; Yesilbag, Y.O.; Ertugrul, M. Synthesis of In₂O₃ Nanostructures with Different Morphologies as Potential Supercapacitor Electrode Materials. *Appl. Surf. Sci.* **2018**, *427*, 956–964. [[CrossRef](#)]
22. Zhu, B.; Wu, X.; Liu, W.J.; Lu, H.L.; Zhang, D.W.; Fan, Z.; Ding, S.J. High-Performance On-Chip Supercapacitors Based on Mesoporous Silicon Coated with Ultrathin Atomic Layer-Deposited In₂O₃ Films. *ACS Appl. Mater. Interfaces* **2019**, *11*, 747–752. [[CrossRef](#)] [[PubMed](#)]
23. Kumar, R.; Agrawal, A.; Bhuvana, T.; Sharma, A. Porous Indium Oxide Hollow Spheres (PIOHS) for Asymmetric Electrochemical Supercapacitor with Excellent Cycling Stability. *Electrochim. Acta* **2018**, *270*, 87–95. [[CrossRef](#)]
24. Xu, X.; Wu, T.; Xia, F.; Li, Y.; Zhang, C.; Zhang, L.; Chen, M.; Li, X.; Zhang, L.; Liu, Y.; et al. Redox Reaction between Graphene Oxide and in Powder to Prepare In₂O₃/Reduced Graphene Oxide Hybrids for Supercapacitors. *J. Power Sources* **2014**, *266*, 282–290. [[CrossRef](#)]
25. Mishra, R.K.; Ryu, J.H.; Kwon, H.I.; Jin, S.H. Novel Two-Dimensional In₂O₃ Nanodiscs for High-Rate Performance of Solid-State Symmetric Supercapacitors. *Mater. Lett.* **2018**, *218*, 131–134. [[CrossRef](#)]
26. Chang, Y.; Wang, B.; Huo, Y.; Zhai, K.; Liu, L.; Li, P.; Nie, A.; Mu, C.; Xiang, J.; Zhao, Z.; et al. Layered Porous Materials Indium Triphosphide InP₃ for High-Performance Flexible All-Solid-State Supercapacitors. *J. Power Sources* **2019**, *438*, 227010. [[CrossRef](#)]

27. Hussain, I.; Hussain, T.; Lamiel, C.; Zhang, K. Turning Indium Oxide into High-Performing Electrode Materials via Cation Substitution Strategy: Preserving Single Crystalline Cubic Structure of 2D Nanoflakes towards Energy Storage Devices. *J. Power Sources* **2020**, *480*, 228873. [[CrossRef](#)]
28. Aval, L.F.; Ghoranneviss, M.; Pour, G.B. Graphite Nanoparticles Paper Supercapacitor Based on Gel Electrolyte. *Mater. Renew. Sustain. Energy* **2018**, *7*, 1–11. [[CrossRef](#)]

Disclaimer/Publisher's Note: The statements, opinions and data contained in all publications are solely those of the individual author(s) and contributor(s) and not of MDPI and/or the editor(s). MDPI and/or the editor(s) disclaim responsibility for any injury to people or property resulting from any ideas, methods, instructions or products referred to in the content.